Preprint
UCRL-JC-135092

Core-Level Satellites and Outer Core-Level Multiplet Splitting in Mn Model Compounds

A.J. Nelson, J.G. Reynolds, J.W. Roos

This article was submitted to
46th American Vacuum Society Symposium, Seattle, WA, October 25-29, 1999

October 18, 1999

CORE-LEVEL SATELLITES AND OUTER CORE-LEVEL MULTIPLET SPLITTING IN Mn MODEL COMPOUNDS

A. J. Nelson and John G. Reynolds
University of California
Lawrence Livermore National Laboratory, Livermore, CA 94550

and

Joseph W. Roos
Ethyl Corporation, Richmond, VA 23217

Abstract

We report a systematic study of the Mn 2p, 3s and 3p core-level photoemission and satellite structures for Mn model compounds. Charge-transfer from the ligand state to the 3d metal state is observed and is distinguished by prominent shake-up satellites. We also observe that the Mn 3s multiplet splitting becomes smaller as the Mn oxidation state increases, and that 3s–3d electron correlation reduces the branching ratio of the ^7S:^5S states in the Mn 3s spectra. In addition, as the ligand electronegativity decreases, the spin state purity is lost in the 3s spectra as evidenced by peak broadening. Our results are best understood in terms of the configuration-interaction (CI) model including intrashell electron correlation, charge-transfer and final-state screening.

INTRODUCTION

Photoemission studies on transition metal compounds reveal core-level multiplet structures that are best understood in terms of configuration-interaction (CI) calculations including intrashell electron correlation, charge-transfer and final-state screening.[1-11] In addition, these multiplet structures are also strongly influenced by covalency and ligand coordination.[12,13]

The neutral Mn atom has a $2p^6 3s^2 3p^6 3d^6$ configuration and a high-spin [$3d^5 4s^2$] configuration. The (empty) 4s band lies 2 to 4 eV above the top of the $3d^N$ band, depending on the ion. Transitions are allowed between the initial state $2p^6 3s^2 3p^6 3d^N$ (N = 3,4,5 for Mn^{+4}, Mn^{+3}, Mn^{+2}, respectively) and a series of final states ($2p^5 3d^{N+1}$). Models for satellite structures in the 2p core-level spectra include the shakeup of a valence electron accompanying the photoionization process due to a charge-transfer mechanism from the ligand state to the 3d metal state.[6] For mixing or hybridization of the metal d states with the ligand p states (valence electrons) to occur, the charge transfer states ($d^{N+1}\underline{L}$) should have the same symmetry as the initial d^N state. The charge-transfer energy is defined as the energy required to transfer one electron from the ligand 2p states to the metal 3d states and depends strongly on the ligand electronegativity – the higher the electronegativity, the larger the charge-transfer energy. Since the d-d Coulomb interaction energy and the core hole–d-electron Coulomb attraction energy are primarily

determined by atomic parameters and, thus independent of ligands, it follows that the largest influence on satellite structure would be due to charge-transfer.

It has been shown that for Mn dihalides, the outer Mn 3s core-level final state configuration can be either $\underline{3s}3d^5$ or $\underline{3s}3d^6\underline{L}$ depending on final state screening effects due to the ligand ($\underline{3s}$ and $\underline{L}$ indicate that there is one electron missing in the Mn 3s and the ligand valence state, respectively). Also, the 3s final state has ^7S and ^5S symmetry, e.g. the Mn^{2+} initial state $(3s^23p^63d^5)^6S$ has two possible final states, $(3s^13p^63d^5)^7S$ or $(3s^13p^63d^5)^5S$. In the ^7S state, the remaining 3s electron is well correlated with 3d electrons of parallel spin, while in the ^5S state the two spins are antiparallel. This electron correlation reduces the branching ratio of the ^7S:^5S states. In addition, as the ligand electronegativity decreases, charge-transfer satellites become important and the spin state purity is lost in the 3s spectra. The spectra become representative of mixed unscreened ($3d^N$) and locally screened ($3d^{N+1}$) final states. Thus, we see that the 3s core-level is polarized by the $3d^5$ shell.

This paper presents the results of a systematic study of the 2p, 3s and 3p core-level photoemission, and satellite structures for Mn model compounds. Core-level satellite structure and outer core-level multiplet splitting were characterized as a function of ligand electronegativity. Interpretation of the 2p, 3p and 3s spectra is consistent with the configuration-interaction (CI) model including intrashell electron correlation, charge-transfer and final-state screening.

EXPERIMENTAL

The model compounds MnO, Mn_2O_3, Mn_3O_4, MnO_2, $MnPO_4$, $Mn_5(PO_4)_2[PO_3(OH)]_2 \cdot 4H_2O$ (Alfa Aesar), MnS (Aldrich), $MnSO_4 \cdot H_2O$ (Mallinckrodt), $Mn(OCH_3)_2$ and $Mn(C_5H_7O_2)_3$ (Aldrich) were used as received and pressed into In foil for analysis. For these ionic and covalent model compounds, Mn is either in tetrahedral or octahedral coordination. Table I summarizes the oxidation states and stereochemistry of the Mn model compounds. It should be noted that ligand electronegativity decreases from O^{2-} to SO_4^{2-} to S^{2-} to PO_4^{3-} . The $(OCH_3)^-$ and $(C_5H_7O_2)^-$ ligands are covalently bound to the Mn.

ESCA experiments were performed on a Physical Electronics 5400 ESCA system using Mg Kα radiation (1253.6 eV) and a hemispherical analyzer pass energy of 17.90 eV giving an overall energy resolution of 1.1 eV. Binding energies were referenced to the C 1s photoelectron line arising from adventitious carbon at 284.6 eV.

RESULTS AND DISCUSSION

Figure 1 presents the Mn 2p spectra for the set of model compounds. The binding energy positions for the Mn $2p_{3/2,1/2}$ spin-orbit components range between 641–643 eV and 654–655 eV, respectively, in agreement with literature values[14-17] and are summarized in Table II. The full width half-maximum (FWHM) of the Mn $2p_{3/2}$ peak is 2.5–3.4 eV for these powdered samples. One distinguishing feature of all the Mn^{+2} species in the

phosphates and sulfate is the prominent shake-up satellite about 5 eV higher than the Mn $2p_{3/2}$ peak and is due to charge-transfer.[6] In addition, this satellite-main peak splitting varies approximately as the ligand valence binding energy.

The Auger parameters are also listed in Table I. For the oxide standards, the Auger parameter becomes less negative with increasing oxidation. The Auger parameter for phosphates and sulfates are clustered around -31 eV. Figure 2 shows a plot of the Mn $2p_{3/2}$ binding energy versus the Mn LMM Auger kinetic energy. The Auger parameter plots are useful for further separation of the Mn chemical states and clearly show the phosphates and sulfates clustered in the left bottom corner between $\alpha = -30.6$ and -31.6, away from the oxides.

Understanding the Mn 2p final states ($2p^5 3d^{N+1}$) requires knowledge of the 3d core-level in the valence band. The 3d level in an octahedral coordination (e.g. Mn oxides) is split into higher energy doubly degenerate (e_g) and lower energy triply degenerate (t_{2g}) levels by the crystal field. In contrast, the 3d level in a tetrahedral coordination (e.g. $MnSO_4$) is split into higher energy triply degenerate (t_{2g}) and lower energy doubly degenerate (e_g) levels by the crystal field. The energy difference between the two levels is determined by the strength of the crystal potential and is larger for the octahedral case. If the interaction between the 2p core hole and the correlated 3d valence electrons is sufficiently strong, satellites accompanying the main lines are present in the photoemission spectra. As stated, we observe this satellite feature to varying degrees for

the phosphates and sulfates having tetrahedral coordination. In addition, since the P 3p and S 3p states in the valence band share the same principal quantum number as the Mn 3d states, their overlap will be the largest. The oxides with octahedral coordination (O 2p states in the valence band) do not exhibit this satellite feature.

Figure 3 shows the entire Mn 3p and 3s spectral region for the model compounds. As previously stated, the excitation energy was 1253.6 eV, and thus the positions and relative intensities of the Mn 3s and Mn 3p multiplets can be considered to be in the sudden limit approximation[2,3] with little coupling between the ion and the photoelectron. The figure clearly shows a chemical shift of the Mn $3p_{3/2,1/2}$ spin-orbit pair associated with the Mn 2+, 3+ and 4+ oxidation states. The 3p peaks are somewhat broadened, but a direct correspondence can be made between observed features in these spectra and those in the literature.[10,11] Specifically, the main 3p line represents the ^7P ionic final state and the higher binding energy shoulder represents the spin-orbit component $^5P(1)$. The spectrum for $Mn(OCH_3)_2$ has a stronger than usual feature 6.6 eV from the main peak representative of $^5P(2)$. Also, the broad feature ≈20 eV from the main 3p peak in all the spectra is attributed to an energy-loss peak.

Figure 4 shows the expanded Mn 3s region for the model compounds. The binding energy positions for the Mn 3s ^7S and ^5S multiplet components range between 81–83 eV and 87–89 eV, respectively, and are summarized in Table III. Figure 5 graphically summarizes the Mn oxidation state versus Mn 3s multiplet splitting for the

Mn model compounds. Note that the Mn 3s multiplet splitting (ΔMn 3s) becomes smaller as the Mn oxidation state increases, consistent with published data, except for the $MnPO_4$, which is anomalously high. The polarization of the $-PO_4$ ligand may account for this anomalous behavior since it would draw more charge from the Mn atom. Also note that the ^7S and ^5S multiplet components shift considerably since it involves the binding energy of a ligand valence electron. As previously stated, as the ligand electronegativity decreases, charge-transfer satellites become important and the spin state purity is lost in the 3s spectra. Broadening of the 3s peaks would result as we observe for the PO_4^{3-} ligand having the lowest electronegativity. The covalently bound ligands $(OCH_3)^-$ and $(C_5H_7O_2)^-$ also exhibit broader than usual 3s peaks. The multiplet splitting for these ligands are quite different indicating their polarizations are different. As in the case of the $-PO_4$ ligand, the multiplet splitting for the $-(acac)_3$ ligand is high. The strong polarization of this ligand withdraws mobile π electrons from the Mn atom thus affecting the multiplet splitting.

CONCLUSIONS

We have presented the results of a systematic study of the Mn 2p core-level satellite structure and the Mn 3s and 3p outer core-level multiplet splitting of Mn model compounds as a function of ligand electronegativity. The satellite structure observed in the Mn 2p spectra is clearly associated with ligand 2p to Mn 3d charge-transfer based on sound theoretical arguments and previous experimental work. Also, the Mn 3s multiplet

splitting became smaller as the Mn oxidation state increased. The atomic calculations of Bagus, Freeman and Sasaki[2] including configuration interaction (CI) and correlation in the final states best describes the observed multiplet splitting. The interpretation of the 2p and 3s spectra for these model compounds are thus consistent and complementary.

Acknowledgments

This work was performed under the auspices of the U.S. Department of Energy under Contract W-7405-ENG-48 at LLNL.

References

1. S.P. Kowalczyk, L. Ley, R.A. Pollack, F.R. McFeely and D.A. Shirley, Phys. Rev. **B7**, 4009 (1973).
2. P.S. Bagus, A.J. Freeman and F. Sasaki, Phys. Rev. Lett. **30**, 850 (1973).
3. C.S. Fadley, in *Electron Spectroscopy: Theory, Techniques, and Applications,* edited by C.R. Brundle and A.D. Baker (Academic, London, 1978) Vol. II, Chap. 1.
4. G. van der Laan, C. Westra, C. Haas and G.A. Sawatzky, Phys. Rev. **B23**, 4369 (1981).
5. J. Zaanen, C. Westra and G.A. Sawatzky, Phys. Rev. **B33**, 8060 (1986).
6. Jaehoon Park, Seungoh Ryu, Moon-sup Han and S.-J. Oh, Phys. Rev. **B37**, 10867 (1988).
7. Geunseop Lee and S.-J. Oh, Phys. Rev. **B43**, 14674 (1991).
8. S.-J. Oh, Gey-Hong Gweon and Je-Geun Park, Phys. Rev. Lett. **68**, 2850 (1992).
9. Gey-Hong Gweon, Je-Geun Park and S.-J. Oh, Phys. Rev. **B48**, 7825 (1993).
10. B. Hermsmeier, C.S. Fadley, M.O. Krause, J. Jimenez-Mier, P. Gerard and S.T. Manson, Phys. Rev. Lett. **61**, 2592 (1988).
11. B. Hermsmeier, C.S. Fadley, B. Sinkovic, M.O. Krause, J. Jimenez-Mier, P. Gerard, T.A. Carlson, S.T. Manson and S.K. Bhattacharya, Phys. Rev. **B48**, 12425 (1993).
12. M. Fujiwara, T. Matsushita and S. Ikeda, J. Electron Spectroscopy Rel. Phenom. **74**, 201 (1995).

13. B.W. Veal, D.E. Ellis and D.J. Lam, Phys. Rev. **B32**, 5391 (1985).

14. J. F. Moulder, W. F. Stickle, P. E. Sobol and K. D. Bomben, Handbook of X-Ray Photoelectron Spectroscopy, Perkin-Elmer Corporation, Physical Electronics Division, Eden Prairie, MN 55344 (1992).

15. B. R. Strohmeier and D. M. Hercules, J. Phys. Chem. **88**, 4922 (1984).

16. A. Aoki, Japan J. Appl. Phys. **15(2)**, 305 (1976).

17. J. C. Carver, G. K. Schwietzer and T. A. Carlson, J. Chem. Phys. **57(2)**, 973 (1972).

Figure Captions

Figure 1. High-resolution XPS spectra of Mn 2p core levels for the Mn model compounds.

Figure 2. Mn 2p Auger parameter diagram further separating manganese chemical states.

Figure 3. High-resolution XPS spectra of Mn 3p and 3s core levels for the Mn model compounds.

Figure 4. Expanded Mn 3s core level spectra for the Mn model compounds.

Figure 5. Mn oxidation state versus Mn 3s multiplet separation for the Mn model compounds.

Table I. Oxidation States and Stereochemistry of Mn Model Compounds.

Compound	Oxidation State	Coordination Number	Geometry	Crystal System
MnO	Mn^{2+}	6	octahedral	isometric
Mn_2O_3	Mn^{3+}	6	octahedral	monoclinic
Mn_3O_4	Mn^{2+} Mn^{3+}	4 6	tetrahedral octahedral	isometric
MnO_2	Mn^{4+}	6	octahedral	tetragonal
$MnPO_4$	Mn^{3+}	6	octahedral	isometric tetragonal
Hureaulite[a]	Mn^{2+}	4	tetrahedral	
MnS	Mn^{2+}	4	tetrahedral	isometric
$MnSO_4$	Mn^{2+}	4	tetrahedral	monoclinic
$Mn(OCH_3)_2$	Mn^{2+}	4	tetrahedral	
Mn(2,4) Pentanedione[b]	Mn^{3+}	6	octahedral	

a) $Mn_5(PO_4)_2[PO_3(OH)]_2 \cdot 4H_2O$.

b) $Mn(C_5H_7O_2)_3$ or $Mn(acac)_3$

Table II. Values of Binding Energies (in eV) for Manganese Model Compounds.

Sample	Mn $2p_{3/2}$	FWHM[a]	Mn LMM[d]	α[e]	O 1s	S 2p	P 2p
MnO	640.9	3.2	582.9	-29.8	530.0	–	–
Mn_3O_4	641.0	3.2	583.4	-29.2	529.9	–	–
Mn_2O_3	641.2	3.0	583.4	-29.0	529.8	–	–
MnO_2	641.9	2.5	583.6	-28.1	529.5	–	–
$MnPO_4$	641.9	3.3	581.0	-30.7	531.8	–	134.0
Hureaulite[b]	641.6	3.4	581.2	-30.8	531.5 532.8	–	133.6
$MnSO_4$	641.9	3.3	581.1	-30.6	532.2	168.8	–
MnS	640.5	3.2	584.3	-28.8	–	161.7	–
$Mn(OCH_3)_2$	642.3	3.0	–	–	529.5 533.9	–	–
Mn(2,4) Pentanedione[c]	641.2	3.3	–	–	531.2	–	–

a) Full width half-maximum of Mn $2p_{3/2}$ peak in eV.

b) $Mn_5(PO_4)_2[PO_3(OH)]_2 \cdot 4H_2O$.

c) $Mn(C_5H_7O_2)_3$ or $Mn(acac)_3$

d) Kinetic energy of Mn $L_3M_{2,3}M_{4,5}$ Auger peak.

e) Auger parameter, α = BE + KE – 1253.6 eV.

Table III. Summary of the Mn 3s Photoelectron Results for Manganese Model Compounds.

Sample	Mn 3s (eV)		FWHM[a]		ΔMn 3s (eV)	Mn 3s Branching Ratio[b]
	^7S	^5S	^7S	^5S		
MnO	81.4	87.0	3.2	3.4	5.6	1.5
Mn_3O_4	81.6	87.2	3.7	3.7	5.6	1.5
Mn_2O_3	82.1	87.5	3.2	3.8	5.4	1.4
MnO_2	83.0	87.5	3.4	3.8	4.5	1.4
$MnPO_4$	82.6	88.5	5.1	3.8	5.9	1.8
Hureaulite[c]	81.7	87.9	3.3	3.3	6.2	1.7
$MnSO_4$	82.5	88.7	3.3	3.5	6.2	1.7
MnS	81.0	86.9	3.5	5.5	5.9	1.1
$Mn(OCH_3)_2$	82.8	88.3	3.3	4.2	5.4	1.5
Mn(2,4) Pentanedione[d]	82.6	88.7	4.0	4.2	6.1	1.4

a) Full width half-maximum of Mn 3s peaks in eV.

b) The branching ratio of the Mn 3s peaks are based on peak areas, i.e. area ratio of the ^7S:^5S states.

c) $Mn_5(PO_4)_2[PO_3(OH)]_2 \cdot 4H_2O$.

d) $Mn(C_5H_7O_2)_3$ or $Mn(acac)_3$

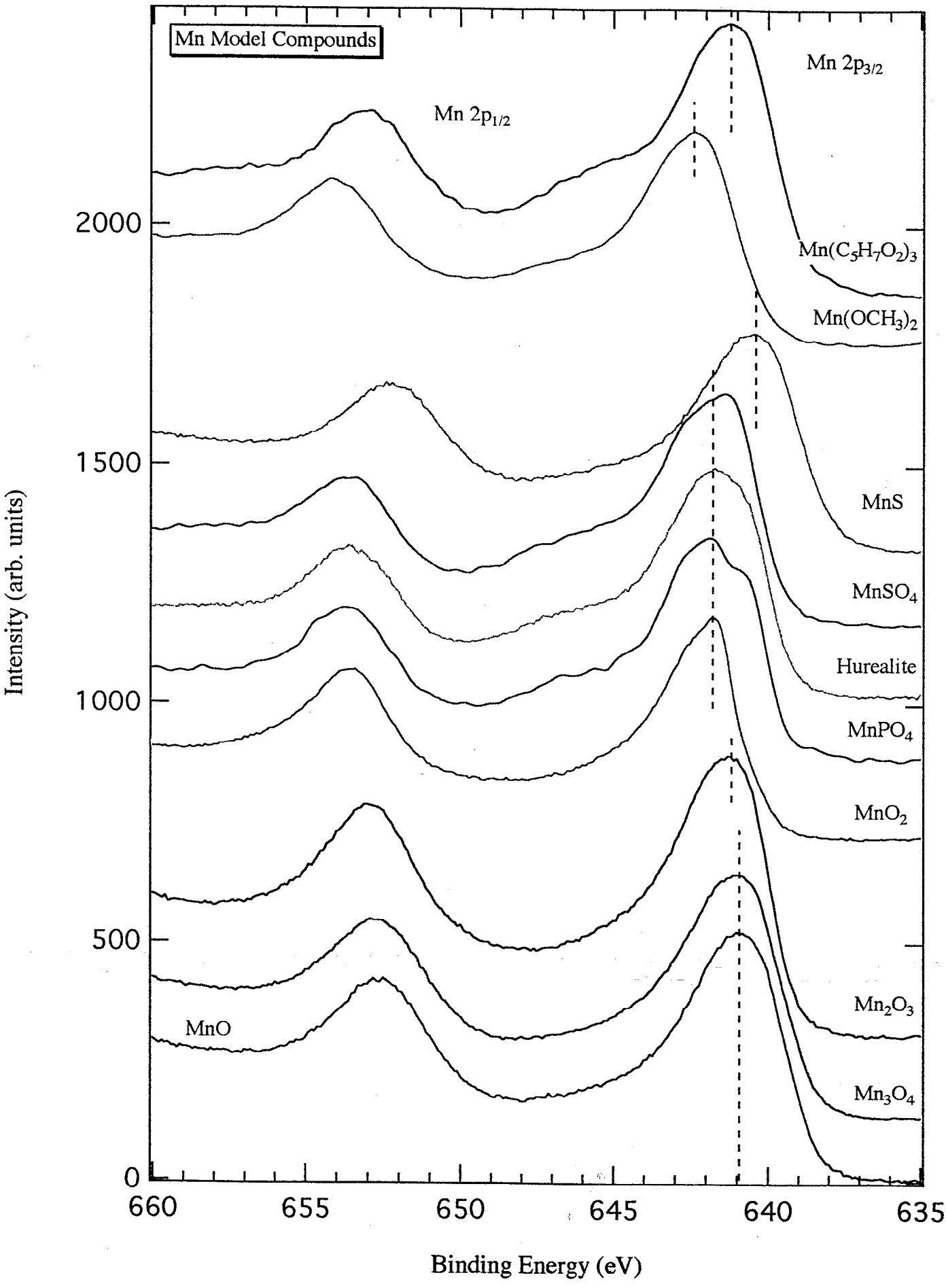
Mn Model Compounds
Mn 2p3/2
Mn 2p1/2
Mn(C5H7O2)3
Mn(OCH3)2
MnS
MnSO4
Hurealite
MnPO4
MnO2
Mn2O3
Mn3O4
MnO
Intensity (arb. units)
2000
1500
1000
500
0
660
655
650
645
640
635
Binding Energy (eV)

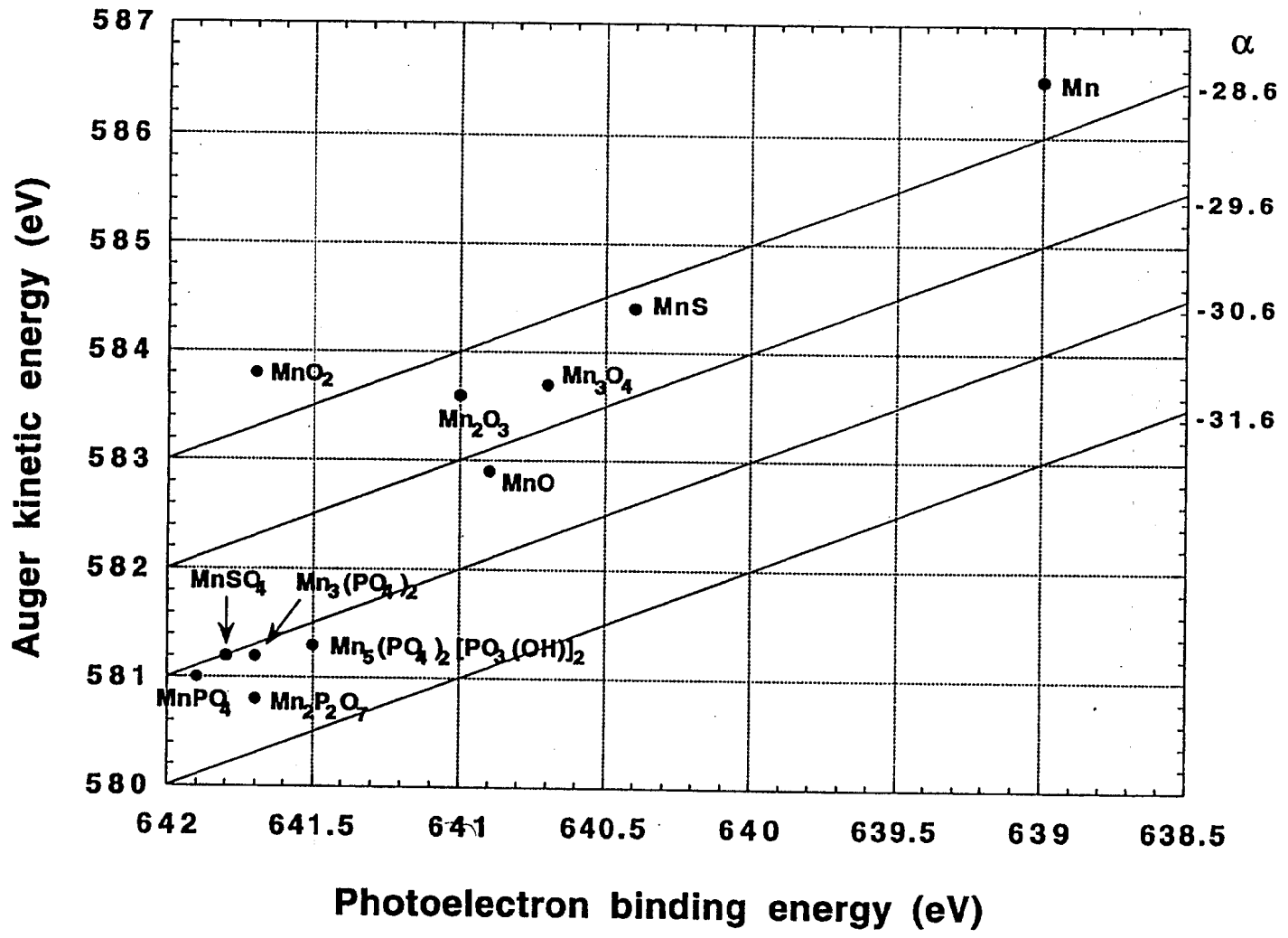
Auger kinetic energy (eV)
587
586
585
584
583
582
581
580
642
641.5
641
640.5
640
639.5
639
638.5
Photoelectron binding energy (eV)
α
-28.6
-29.6
-30.6
-31.6
Mn
MnS
MnO2
Mn3O4
Mn2O3
MnO
MnSO4
Mn3(PO4)2
Mn5(PO4)2[PO3(OH)]2
MnPO4
Mn2P2O7

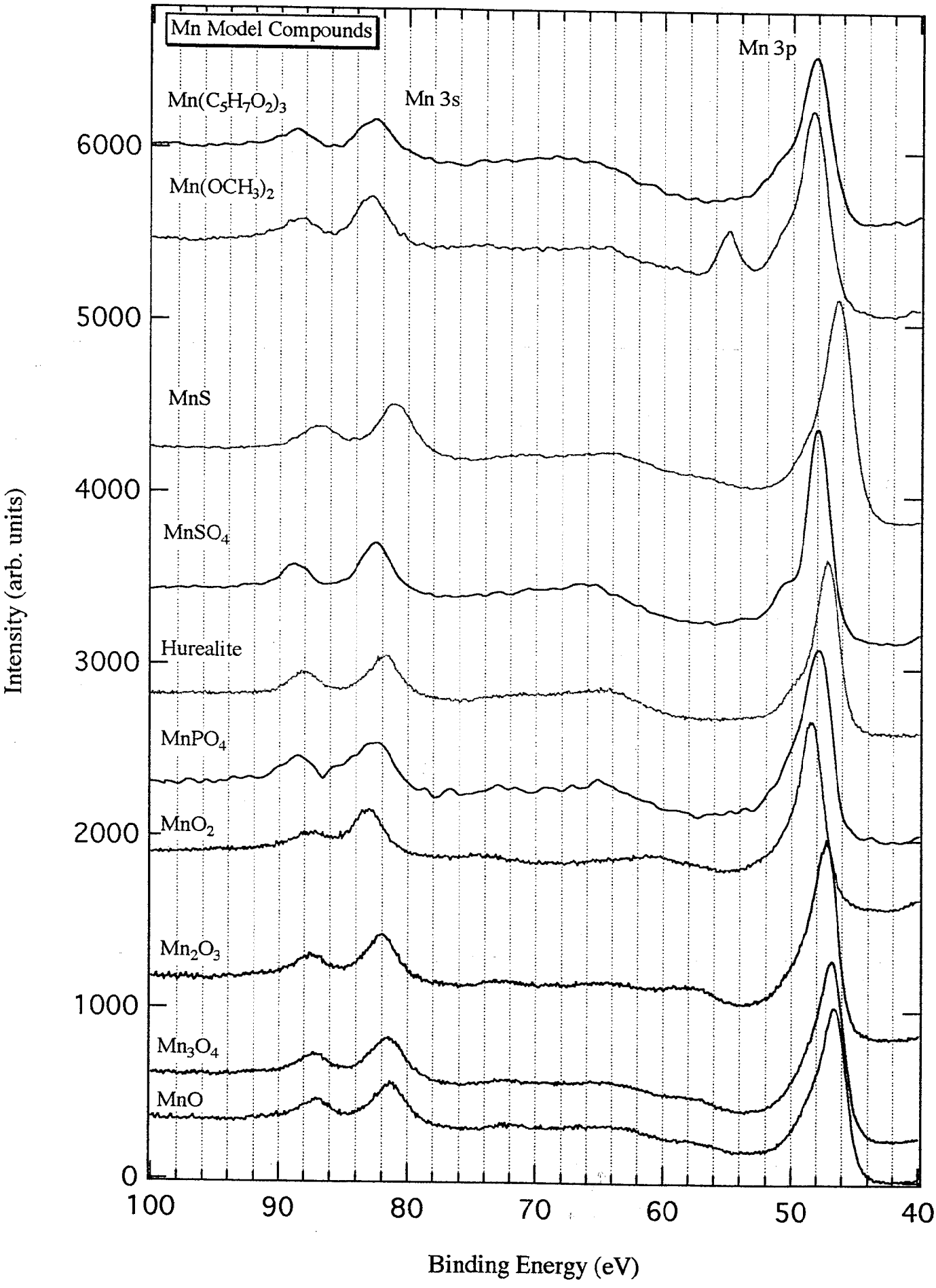
Mn Model Compounds
Mn 3p
Mn 3s
$Mn(C_5H_7O_2)_3$
$Mn(OCH_3)_2$
MnS
$MnSO_4$
Hurealite
$MnPO_4$
MnO_2
Mn_2O_3
Mn_3O_4
MnO
Intensity (arb. units)
0
1000
2000
3000
4000
5000
6000
100
90
80
70
60
50
40
Binding Energy (eV)

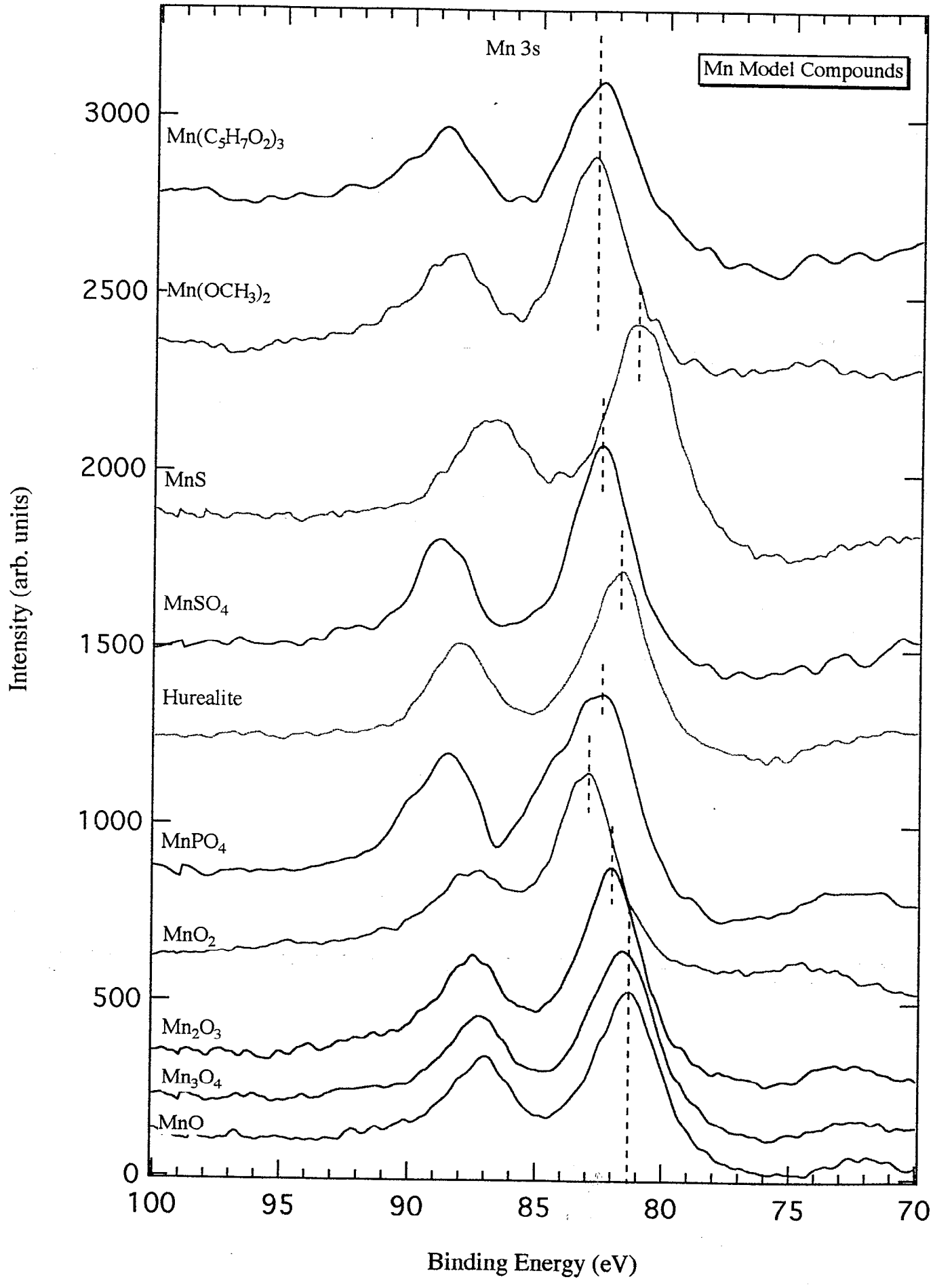
Mn 3s
Mn Model Compounds
3000
2500
2000
1500
1000
500
0
Mn(C5H7O2)3
Mn(OCH3)2
MnS
MnSO4
Hurealite
MnPO4
MnO2
Mn2O3
Mn3O4
MnO
100
95
90
85
80
75
70
Intensity (arb. units)
Binding Energy (eV)

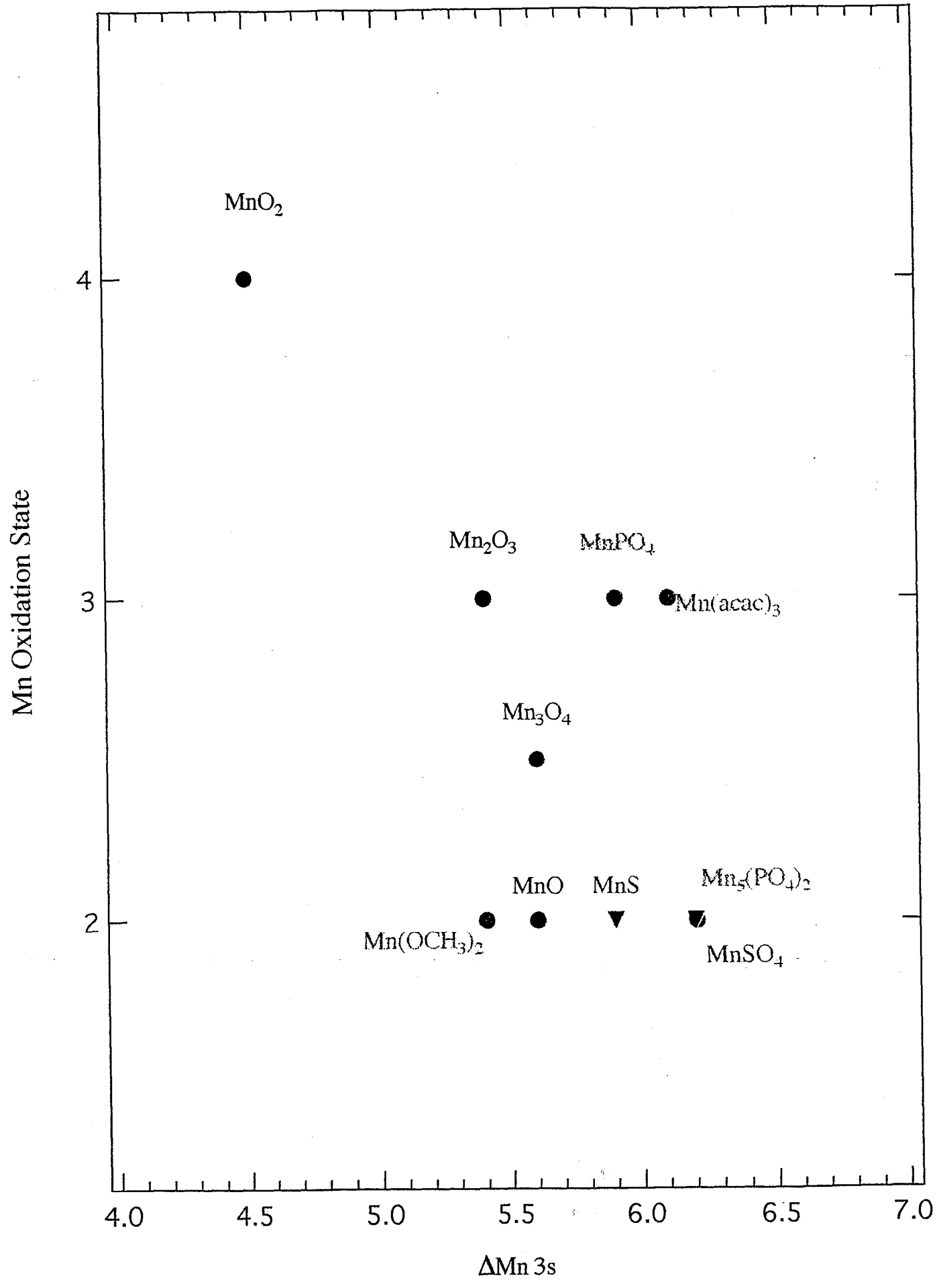
MnO2
Mn2O3
MnPO4
Mn(acac)3
Mn3O4
MnO
MnS
Mn5(PO4)2
Mn(OCH3)2
MnSO4
Mn Oxidation State
4
3
2
4.0
4.5
5.0
5.5
6.0
6.5
7.0
ΔMn 3s